Ion-Specific Effects under Confinement: The Role of Interfacial Water

Dimitrios Argyris,[†] David R. Cole,[‡] and Alberto Striolo[†,*]

[†]The University of Oklahoma School of Chemical, Biological, and Materials Engineering, Norman, Oklahoma 73019 and [‡]Oak Ridge National Laboratory Geochemistry and Interfacial Science Group, Chemical Sciences Division, Oak Ridge, Tennessee 37831-6110

ABSTRACT All-atom molecular dynamics simulations were employed for the study of the structure and dynamics of aqueous electrolyte solutions within slit-shaped silica nanopores with a width of 10.67 Å at ambient temperature. All simulations were conducted for 250 ns to capture the dynamics of ion adsorption and to obtain the equilibrium distribution of multiple ionic species (Na^+, Cs^+, and Cl^-) within the pores. The results clearly support the existence of ion-specific effects under confinement, which can be explained by the properties of interfacial water. Cl^- strongly adsorbs onto the silica surface. Although neither Na^+ nor Cs^+ is in contact with the solid surface, they show ion-specific behavior. The differences between the density distributions of cations within the pore are primarily due to size effects through their interaction with confined water molecules. The majority of Na^+ ions appear within one water layer in close proximity to the silica surface, whereas Cs^+ is excluded from well-defined water layers. As a consequence of this preferential distribution, we observe enhanced in-plane mobility for Cs^+ ions, found near the center of the pore, compared to that for Na^+ ions, closer to the solid substrate. These observations illustrate the key role of interfacial water in determining ion-specific effects under confinement and have practical importance in several fields, from geology to biology.

KEYWORDS: molecular dynamics simulation · solid−liquid interfaces · silica · SPC/E water · ions · aqueous electrolytes

The understanding of aqueous electrolyte solutions near charged surfaces continues to attract great attention due to recent advances in nanofabrication[1−3] and a wide range of applications including nanofluidics and "lab-on-chip" processes,[4−7] manipulation of biological membranes and ion channels,[8,9] design of ion-exclusion processes, and desalination membranes.[10−12] The development of nanoporous materials for any of these applications requires a detailed molecular-level understanding of solvent−electrolyte behavior at interfaces and under confinement. Additionally, a predictive understanding of fluid−matrix interactions in subsurface systems also requires insights into phenomena operating at the atomistic and molecular scales.[13]

Computer simulation studies have been used extensively to describe the structural properties of water near solid surfaces at various temperature and pressure conditions.[14−22] The dynamic behavior of interfacial water has also been investigated for a number of systems.[23−26] The results of these investigations support the conclusion that interfacial water properties differ significantly from those observed in the bulk. A number of experimental studies confirmed the predicted behavior. Such studies include backscattering spectroscopy,[27] quasi-elastic neutron scattering,[28] attenuated total reflectance infrared spectroscopy,[29] X-ray reflectivity measurements,[30] and ultrafast infrared spectroscopy.[31]

For most of the applications mentioned above, the fluid systems contain water with electrolytes. We demonstrate herein that understanding the properties of pure interfacial water is essential for accurately describing ion distributions under confinement.

Our current theoretical understanding of aqueous electrolyte solutions at interfaces is not well-developed. The classical Poisson−Boltzmann (PB) approach is hampered by the mean-field approximation and the infinitesimal description of ions it implements, which could lead to an unsatisfactory description of the electric double layer. At short distances from a charged surface, the PB prediction for ion distributions cannot be accurate due to the finite size ion effects[32] and also because of the molecular nature of water,[33] as shown by the Monte Carlo simulation results reported by Yang *et al.*[34] The assumption of uniform surface charge density may also lead to unrealistic predictions of the distributions of ions at interfaces. A promising approach to describe ion distribution at interfaces has recently been used by Tavares *et al.*[35] This mean-field approach requires

knowledge of the local value for the dielectric constant, generally not available.

Unlike the theoretical approaches just summarized, molecular simulations can explicitly account for the molecular nature of both ions and water, and they can also treat surfaces with atomically detailed precision, thus yielding heterogeneous distributions of surface charges where appropriate. Although long simulation times are required to achieve properly equilibrated states, the growing interest in ion-exclusion processes, ion selectivity, and ion transport through pores and membranes justifies attempting atomistic simulations for realistic systems.[36–40] Shirono et al.[41] employed Monte Carlo and molecular dynamics simulations to study KCl distribution and transport in silica nanopores that contain both hydrophobic and hydrophilic surface patches. Their results suggest adsorption of Cl^- at the silica walls and diffusion of K^+ through the center of the hydrophilic pore region. Similar computational studies conducted for various electrolyte solutions on a goethite (α-FeOOH) surface have shown the importance of the molecular structure of interfacial water in determining the distribution of ions near the solid substrate.[42] Marry et al.[43] showed that the nature of counterions does not significantly alter the structure and dynamics of water near a clay surface.

A large body of literature exists describing the properties of bulk electrolyte solutions that provide the foundation for comparisons with behavior of confined fluids. For example, Lee et al.[44] used molecular dynamics simulations to study the mobility and hydration numbers of alkali metal ions and halides at ambient temperature. Diffusion coefficients[45] for Na^+ and Cl^- and the solubility of NaCl and KF in water have been reported at different temperatures by Sanz and Vega.[46] The effect of salt concentration on ionic structural and transport properties of aqueous CsCl solutions have been described by Du et al.[47]

In this study, we report structural and dynamic behavior of aqueous electrolyte solutions under nanoscale confinement. We employed equilibrium all-atom molecular dynamics simulations to study aqueous systems confined within a positively charged silica nanopore with a width of 10.67 Å. Because simulations conducted on thin water films show that the water−structure perturbation at the interface persists for about 10 Å from the substrate, the pore width considered here ensures that the structure of the confined solution is perturbed simultaneously by both surfaces. After allowing for extensive equilibration times, we calculated density profiles and mobilities for the confined ions. The results clearly demonstrate the existence of ion-specific effects under confinement. More importantly, however, we found that by describing the structure and dynamics of water we could adequately explain all of our results, suggesting that water−ion correlations cannot be overlooked when a detailed pre-

diction of ionic behavior is required, especially under nanoscale confinement.

SIMULATION DETAILS

Slit-shaped nanopore configurations were used in our simulations. Two silica substrates with identical surfaces were placed at a distance of 10.67 Å along the z-axis. The (111) crystallographic face of β-cristobalite[48] was used to model the solid substrate. The surface area of each periodic system is 104.8 × 100.8 Å^2 (x−y plane) with a plate thickness of 10.3 Å; details on the surface preparation can be found elsewhere.[49] To obtain a chemically realistic surface, all of the nonbridging oxygen atoms are hydroxylated. The resulting surface hydroxyl group density is ~4.5 OH/nm^2, which corresponds to experimental densities observed on silica surfaces.[50] The surface charge density of the simulated surface is 0.31 C/m^2. The CLAYFF force field[51] was implemented to model the surface. The silicon and oxygen atoms were held at fixed positions, while the surface hydrogen atoms were allowed to vibrate and thus account for momentum exchange between aqueous solution and surface. We did not account for surface reconstruction or silanol deprotonation. The rigid SPC/E water model was used to describe water. This model is known to adequately reproduce experimentally observed structural and dynamic properties, such as pair correlations and diffusion coefficients at ambient conditions.[52] Bond lengths and angles for water molecules were kept fixed using the SETTLE algorithm.[53] Nonbonded interactions were modeled by means of dispersive and electrostatic forces. The van der Waals interactions were treated according to the 12−6 Lennard-Jones (LJ) potential. The LJ parameters for unlike interactions were obtained using the Lorentz−Berthelot mixing rules from pure component ones.[54] The electrostatic forces were described by a Coulombic potential with a cutoff set to 9 Å. Long-range interactions were calculated by the particle mesh Ewald (PME) method.[55] All simulations were performed in the NVT ensemble.[54]

Three different electrolyte solutions, each including 3570 water molecules, were confined between the two identical silica substrates. The three electrolyte mixtures consisted of 64 pairs of either NaCl or CsCl and 32 pairs of both NaCl and CsCl, respectively. The ionic strength in all of the systems was 1 M. The potential parameters for sodium (Na^+), cesium (Cs^+), and chloride (Cl^-) ions were fitted for the SPC/E water model by Dang and collaborators to reproduce accurately the bulk properties.[56,57] The parameters have been used previously to study ion mobility in water[44] and ion adsorption at solid−liquid interfaces.[58] The system temperature was maintained at 300 K by using the Nosé−Hoover thermostat[59,60] with a relaxation time of 100 fs. Periodic boundary conditions were applied in the three directions. The equations of motion were

solved using the molecular dynamics package GROMACS,[61−63] by implementing the leapfrog algorithm[64] with a time step of 1.0 fs. The total simulation time for all cases was 250 ns (250 × 10⁶ time steps). Only the last 40 ns were used to calculate the properties of interest. We found that long simulations are necessary to obtain reliable results.

RESULTS AND DISCUSSION

Cation−Anion Distributions. A side view of the slit-shaped silica pore with the 64 pairs of NaCl ions is shown in Figure 1a. The pore width of 10.67 Å is defined by the distance between the two planes of nonbridging oxygen atoms facing across the pore volume. This simulation snapshot is taken after 250 ns of simulation time. Sodium and chloride ions are presented as purple and green spheres, respectively; water molecules are not shown for clarity. In this figure, we observe the adsorption of Cl^- on the positively charged silica surface and the distribution of Na^+ throughout the pore width. Similar qualitative observations are valid for the CsCl solution. Further, we observe a noticeable reorientation of the surface hydroxyl groups associated with Cl^- ion adsorption, as shown in Figure 1b. This reorientation demonstrates that accounting for the heterogeneous distribution of surface charged sites is crucial for obtaining a realistic description of the ionic distribution accurate at the atomic level.

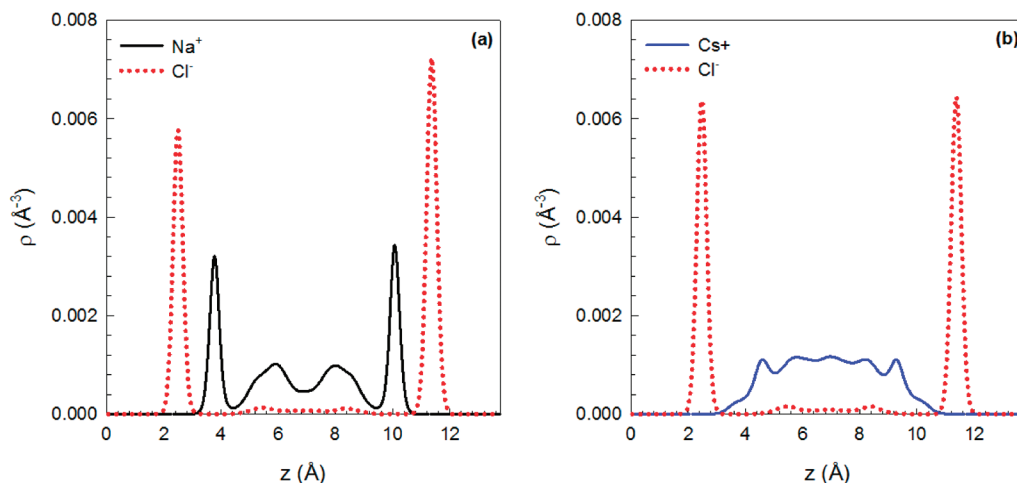The ion density profiles for NaCl and CsCl solutions are presented in Figure 2a,b, respectively. The reference plane ($z = 0$) for all calculations is the lower innermost plane of silicon atoms (brown spheres in Figure 1a). The results indicate the formation of two chloride layers in contact with the pore surfaces (peaks at 2.45 and 11.30 Å) for both systems considered. As expected, these results confirm that the positively charged surfaces attract the counterions (Cl^-). We point out that

Figure 1. (a) Side view of the silica pore with a width of 10.67 Å. Na^+ (purple spheres) and Cl^- (green spheres) ions in the silica pore are shown after 250 ns of simulation at 300 K. White, red, and brown spheres represent hydrogen, oxygen, and silicon atoms of the solid substrate, respectively. Water molecules are not shown for clarity. (b) Enlarged detail of one simulation snapshot illustrating one Cl^- ion in contact with the silica surface. Only selected atoms from the solid substrate are shown to illustrate the reorientation of the surface hydroxyl groups near the Cl^- ion.

Figure 2. Atomic density profiles for Na^+, Cs^+, and Cl^- ions as a function of the distance z from the fully hydroxylated silica surfaces. Panels a and b show data for NaCl and CsCl aqueous solutions, respectively. The reference ($z = 0$) for these calculations is the first innermost plane of silicon atoms. All simulations are conducted at $T = 300$ K, and results are obtained as an average during the last 40 ns of the 250 ns simulations.
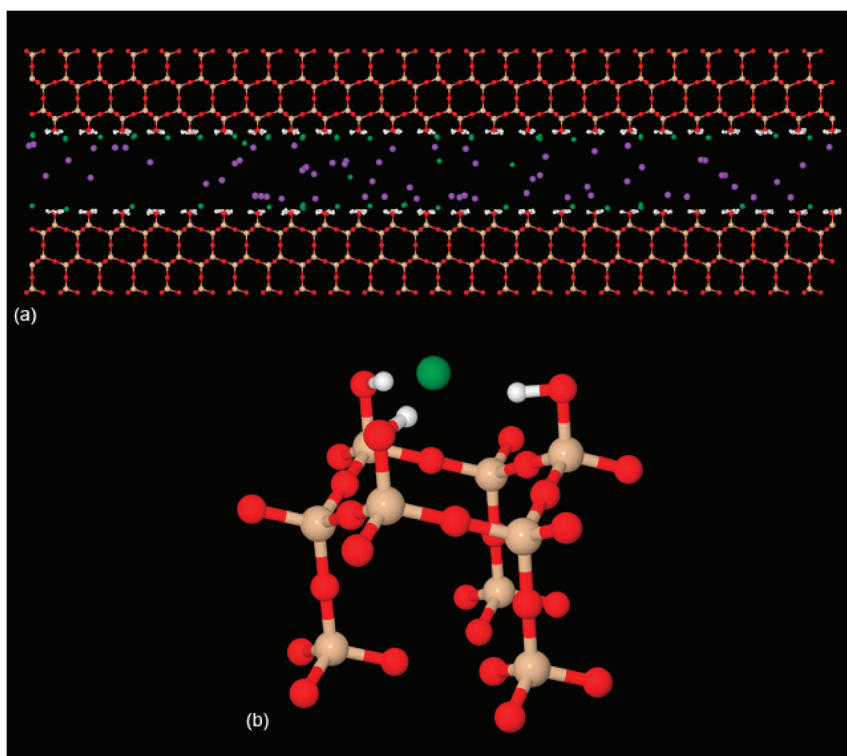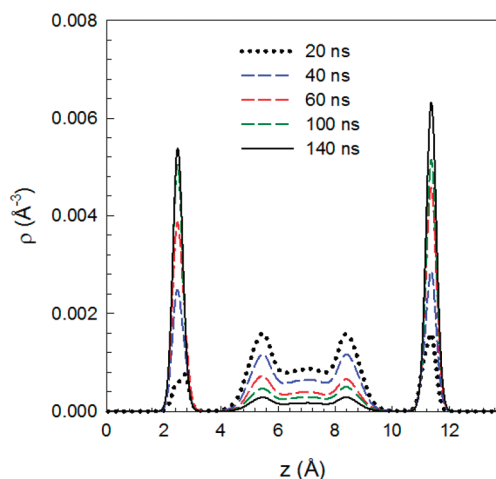
Figure 3. Atomic density profiles for Cl⁻ ions as a function of the distance *z* obtained at different simulation time segments. The data shown are for the system with 64 pairs of NaCl ions. Dotted black line and dashed blue, red, and green, and solid black lines correspond to density profiles at 20, 40, 60, 100, and 140 ns, respectively. Each curve is obtained as an average of simulation results observed during 40 ns of simulation (*e.g.*, data obtained from 60 to 100 ns are shown as the green dashed line labeled "100 ns"). The reference (*z* = 0) for this calculation is the first innermost plane of silicon atoms.

the Cl⁻ layers formed in contact with the SiO₂ surface are rather sparse due to the relatively low Cl⁻ concentration. No significant changes in the density profiles were observed within the last 40 ns of our simulations, but it should be pointed out that adsorbed Cl⁻ ions very rarely desorb from the solid substrate.

The difference in the intensity of the Cl⁻ density peaks near the two solid surfaces exhibited in Figure 2a is due to a slightly higher number of chloride ions adsorbed on the upper pore surface. Note that all ions were initially randomly placed near the pore center. Because the asymmetry observed in Figure 2a is primarily due to the slow adsorption–desorption process with respect to the length of our simulation, simulations far longer than those conducted here are necessary to obtain symmetric distributions for the Cl⁻ ions across the pore. In contrast, the results presented in Figure 2b for the CsCl solution present two equally dense chloride layers near the solid surfaces. To better understand the kinetic effects responsible for the asymmetric density distribution observed in some cases for Cl⁻ ions, the results from different simulation time segments are shown in Figure 3, demonstrating how the Cl⁻ density profile changes as the simulation progresses. These results clearly highlight that long simulations are required to obtain reliable data. Although no significant change in the Cl⁻ density profiles is observed from 100 to 140 ns of simulation (solid black line in Figure 3), we continued our simulation for 250 ns, and only Cl⁻ density data obtained from 210 to 250 ns were used to draw our conclusions. We note that Na⁺ and Cs⁺ ions in all cases reached the equilibrium density profile within the first 20 ns, and no
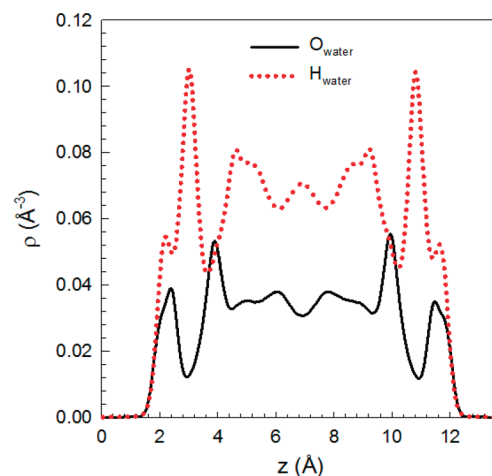

Figure 4. Atomic density profiles for water oxygen and hydrogen atoms as a function of the position *z* across the silica pore. The reference (*z* = 0) is the first innermost plane of silicon atoms. Results are identical in all systems considered in this study.

changes were observed in their density distributions from that point forward. The data in Figure 2 also suggest that a limited number of Cl⁻ ions remain in the center of the pore at specific distances from the two surfaces (~5 Å).

More important for our discussion are the density distributions of cations, for which we report ion-specific behavior. The density data for Na⁺ in Figure 2a suggest the formation of two peaks near each of the pore surfaces. The first pronounced peaks appear at 3.75 Å from the surface, whereas the broader second peaks form at 5.90 Å from each surface. Our results suggest that 76% of Na⁺ ions accumulate at 3.75 Å from the surface and the rest within the central region of the pore. In contrast, the data for Cs⁺ in Figure 2b do not show well-defined density peaks and thus provide no evidence supporting the formation of local structures. We observe only a minimal accumulation occurring at ~4.60 Å, which is in contact with interfacial water layers.

Relation between Water Structure and Ion Distributions. The different density distributions of Na⁺ and Cs⁺ ions within the pores are related to size effects (the diameters of Na⁺ and Cs⁺ are 2.58 and 3.88 Å, respectively, while all other parameters used for these ions remain the same for both simulations) but also to the structure of interfacial water. Numerous simulation studies have reported on the structural and dynamic behavior of interfacial water on silica.[19,20,65,66] In general, highly structured water is observed for up to 10 Å from the solid substrate, and slower dynamics is observed in this interfacial region compared to bulk water. The specific details of this behavior, however, depend on the features of the solid substrate. The water density profiles within the fully hydrated silica nanopores considered in this study are given in Figure 4. The atomic density profile for oxygen shows the formation of two hydration

TABLE 1. Positions of the First Two Atomic Layers for Cations, Anions, and Water Considered in This Study[a]

aqueous electrolyte mixture	atomic species	position of layers (Å)
NaCl—CsCl	Na$^+$	3.75/5.90
	Cs$^+$	4.60/5.75
	Cl$^-$	2.45/~5.45[b]
water	O$^-$	2.35/3.90
	H$^+$	2.20[c]/3.05/4.65

[a]The data reported are for the mixture with 32 pairs of NaCl and CsCl. The same layer positions are observed for the simulated systems with 64 pairs of NaCl or CsCl. The distances given for the atomic layer positions are the same for both surfaces of the nanopores. All distances are given with respect to the innermost plane of the silicon atoms in the nanopore along the z-axis. [b]This distance from the surface corresponds to a weakly pronounced layer of Cl$^-$ in which the anions preferentially accumulate when present in the center of the nanopore. [c]This feature on the density profiles corresponds to a shoulder.

layers near each surface, with peaks appearing at 2.35 and 3.90 Å. Correspondingly, the data for water hydrogen density distribution show the formation of two atomic layers located at 3.05 and 4.65 Å from each surface. The hydrogen density distribution also shows a small shoulder at 2.20 Å, suggesting localized water structuring at the contact with the silica surfaces. Although local perturbations in the water structure near each ion are likely because of ion-hydration phenomena, we note that the differences observed in the averaged water density profiles are negligible when either NaCl or CsCl is in solution and that the density profiles for water are similar to those obtained for pure water, shown in Figure 4. This suggests that the ions considered in this study, at 1 M concentration, do not alter the interfacial water structure significantly. Similar results were reported by Marry et al.[43] for aqueous solutions of NaCl and CsCl confined within clay pores. The positions of all atomic layers are reported in Table 1. The Lennard-Jones size parameters for Na$^+$, Cs$^+$, and water are 2.58, 3.88, and 3.17 Å, respectively. A comparison of results for density profiles suggests that the dense inter-

facial water layer at 3.90 Å plays a significant role in determining the ionic distribution. This water layer appears permeable to Na$^+$ ions, allowing them to being incorporated within its structure (the first Na$^+$ density peak also appears at 3.90 Å). In contrast, Cs$^+$, due to volume-exclusion effects, cannot fit within the well-defined water layer located at 3.90 Å.

Mixed Solute Behavior. In order to evaluate the importance of ion—ion correlations, and the possible competition between Na$^+$ and Cs$^+$ for adsorption sites within the nanopore, a multi-ion mixture was studied by introducing 32 pairs of NaCl and CsCl while keeping the ionic strength at 1 M. Density profiles for solvent—anion and solvent—cation pairs are presented in Figure 5a,b, respectively. We note that the formation of Na$^+$ and Cs$^+$ layers (as shown in Figure 5a) occurs at the same positions as those given in Figure 2a,b for NaCl and CsCl solutions, respectively. The difference in the peak intensities is due to the reduced number of each cation type used for the simulations of mixtures, compared to those used for the results in Figure 2. The incorporation of Na$^+$ and exclusion of Cs$^+$ within the interfacial water layer observed at 3.90 Å becomes more evident in Figure 5a. In Figure 5b, the Cl$^-$ density data are plotted together with those for water oxygen atoms. The formation of one Cl$^-$ layer in contact with the surface is clearly observed and is analogous with the results displayed in Figure 2. At the distance of 2.35 Å, we notice evidence of water structuring. These findings suggest a strong Cl$^-$ surface attraction that is not affected by the repulsive forces that might arise because of the negatively charged water oxygen atomic layer that also forms in contact with the substrate. This is possible because Cl$^-$ ions strongly correlate with the surface hydroxyl groups, as shown in Figure 1b. In contrast, evidence for a strong repulsion of Cl$^-$ due to a pronounced water oxygen layer is observed at 3.90 Å, where the Cl$^-$ density is effectively zero. The interfacial water layer
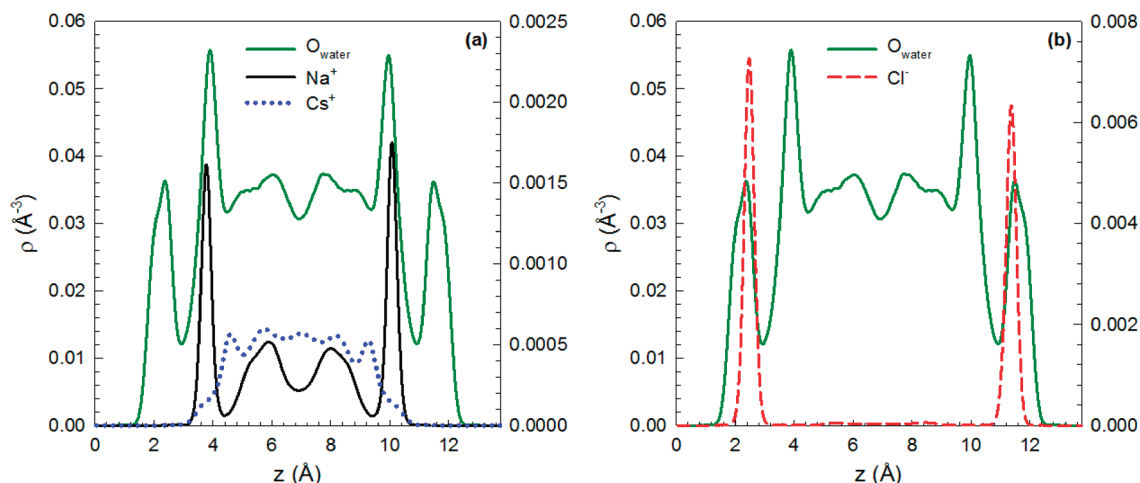

Figure 5. (a) Atomic density profiles of oxygen water with cations (Na$^+$, Cs$^+$) and (b) oxygen water with anions (Cl$^-$) as a function of distance z from the solid surface. The data are shown for the aqueous solution containing both NaCl and CsCl. The reference (z = 0) for these results is the first innermost plane of silicon atoms.
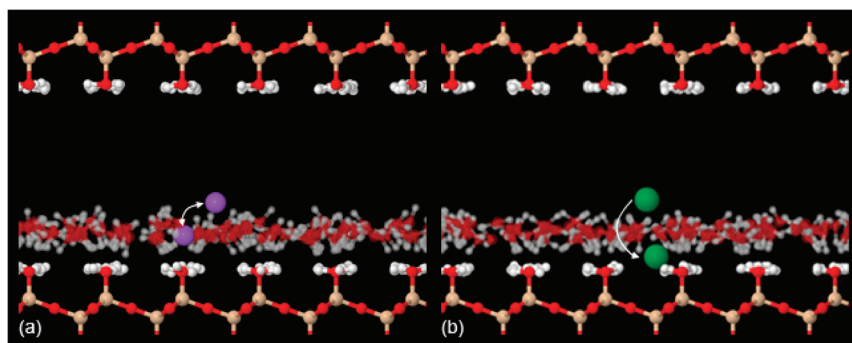
Figure 6. Simulation snapshots illustrating the movement of cations in the silica nanopores. (a) Diffusion of Na$^+$ along its equilibrium positions. (b) Adsorption path for Cl$^-$ on the silica surface. Only the second (at 3.90 Å; see Table 1) layer of interfacial water is shown for clarity.

acts as a kinetic barrier to Cl$^-$ adsorption. The slow transport of Cl$^-$ from the center of the pore to the solid—liquid interface (documented in Figure 3) is related to the slow z-directional mobility of that ion, presumably due to the dense, negatively charged oxygen water layer formed at 3.90 Å from the surface. The slow mobility of Cl$^-$ ions perpendicular to the interface is coupled with slow mobility in the direction parallel to the interface, as described below. Selected snapshots of Na$^+$ and Cl$^-$ are shown in Figure 6, along with the layer of interfacial water formed at 3.90 Å, to schematically illustrate the role of water on the ion distribution at the interface. Na$^+$ ions are easily incorporated within the water layer, and the exchange identified in Figure 6a is consequently fast. On the other hand, Cl$^-$ ions are repelled by the dense, negatively charged interfacial water layer. Consequently, the transport event shown in Figure 6b is kinetically slow.

Dynamics of Confined Water and Ions. Because the in-plane diffusion of interfacial water strongly depends on the distance from a silica surface,[26,67] it is likely that the mobility of the ionic species within our system differs depending on the preferential distribution within
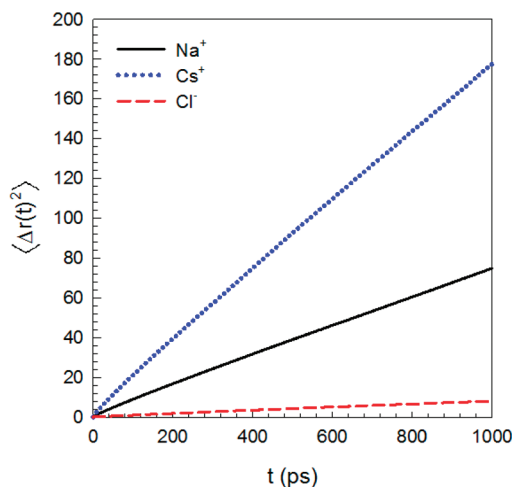

Figure 7. In-plane mean square displacement of Na$^+$, Cs$^+$, and Cl$^-$ in the silica pores. The data are shown for NaCl and CsCl aqueous solutions. The in-plane mean square displacement curve for Cl$^-$ is identical in both systems.

the pore. Namely, it is expected that ions closer to the surface will exhibit slower diffusion. The dynamic behavior for each ionic species was assessed by means of in-plane mean square displacements, calculated along the direction parallel to the solid surface. The results are shown in Figure 7. The data shown were calculated for the systems with 64 pairs of either NaCl or CsCl. No significant difference was observed when the mixed system in which 32 pairs of NaCl and 32 pairs of CsCl were simulated simultaneously.

The results shown in Figure 7 confirm that those ions that are further from the surface (Cs$^+$) move faster than the others. The $x-y$ diffusion coefficients can be evaluated from the slope of the curves shown in Figure 7. The calculated self-diffusion coefficients are ~1.84 × 10^{-6}, 4.37 × 10^{-6}, and 1.98 × 10^{-7} cm^2/s for Na$^+$, Cs$^+$, and Cl$^-$, respectively. These data are consistent with limited in-plane mobility for Cl$^-$, which is in contact with the surface. The larger diffusion coefficient for Cs$^+$ is due to the fact that these cations are found primarily at the center of the nanopore. Simulation results indicate that Na$^+$ ions appear to have slower diffusion than Cs$^+$. This behavior is explained by the incorporation of Na$^+$ in the dynamically hindered hydration layer near the solid surface, where Na$^+$ substitutes for interfacial water molecules.

CONCLUSIONS

Aqueous electrolyte solutions confined within silica nanopores were studied by means of all-atom molecular dynamics simulations. Long (250 ns) molecular dynamics simulations were conducted to reach equilibrium and capture the structural and dynamical aspects of the adsorption process. Three different electrolyte solutions (NaCl, CsCl, and NaCl + CsCl) each with ionic strength of 1 M were simulated at ambient temperature. To assess structural and dynamic behavior of electrolytes, we calculated density profiles and in-plane diffusion coefficients. Strong ion-specific behavior is reported for both equilibrium ion distribution and mobility. We provide evidence according to which the observed difference in mobility for each ionic species is determined by the equilibrium distributions within the pores. We observed that Cl$^-$ ions preferentially adsorb onto the positively charged surfaces, where they associate with the surface hydroxyl groups. Na$^+$ ions are incorporated predominantly into the second adsorbed water layer. The larger Cs$^+$ ions are excluded from the interfacial water layers and for the most part accumulate at the pore center. As a consequence of these preferential ionic distributions, we found that (1) Cl$^-$ mobility is the slowest of all simulated ions because Cl$^-$ ions bond with hydroxyl groups present at the silica surface;

(2) Na^+ ions move faster than Cl^- ions, but because they are strongly incorporated within an interfacial water layer characterized by slow diffusion, their diffusivities are hindered; (3) Cs^+ ions, which predominately accumulate at the pore center, exhibit a self-diffusion coefficient that is more than twice that obtained for Na^+ ions. No significant difference in the structure and dynamics is observed when Na^+ and Cs^+ coexist compared to when either Na^+ or Cs^+ is simulated separately. The above observations suggest that water–ion and silica–ion interactions play primary roles in dictating the ion-specific behavior for the system considered here, while ion–ion correlations have limited influence. Consequently, a deep understanding of the properties of interfacial water appears crucial toward accurately predicting ion-specific effects under confinement.

REFERENCES AND NOTES

1. Mailly, D. Nanofabrication techniques. *Eur. Phys. J.* **2009**, *172*, 333–342.

2. Wu, M.-Y.; Smeets, R. M. M.; Zandbergen, M.; Ziese, U.; Krapf, D.; Batson, P. E.; Dekker, N. H.; Dekker, C.; Zandbergen, H. W. Control of shape and material composition of solid-state nanopores. *Nano Lett.* **2009**, *9*, 479–484.

3. Quake, S. R.; Scherer, A. From micro- to nanofabrication with soft materials. *Science* **2000**, *290*, 1536–1540.

4. Plecis, A.; Schoch, R. B.; Renaud, P. Ionic transport phenomena in nanofluidics: experimental and theoretical study of the exclusion-enrichment effect on a chip. *Nano Lett.* **2005**, *5*, 1147–1155.

5. Noy, A.; Park, H. G.; Fornasiero, F.; Holt, J. K.; Grigoropoulos, C. P.; Bakajin, O. Nanofluidics in carbon nanotubes. *Nano Today* **2007**, *2*, 22–29.

6. Schoch, R. B.; Han, J. Y.; Renaud, P. Transport phenomena in nanofluidics. *Rev. Mod. Phys.* **2008**, *80*, 839–883.

7. Mortensen, N. A.; Xiao, S. S.; Pedersen, J. Liquid-infiltrated photonic crystals: enhanced light-matter interactions for lab-on-a-chip applications. *Microfluid. Nanofluid.* **2008**, *4*, 117–127.

8. Hille, B. *Ion Channels of Excitable Membranes*; Sinauer Associates Inc: Sunderland, MA, 2001.

9. Jiang, Y.; Lee, A.; Chen, J.; Cadene, M.; Chait, B. T.; MacKinnon, R. Crystal structure and mechanism of a calcium-gated potassium channel. *Nature* **2002**, *417*, 515–522.

10. Fornasiero, F.; Park, H. G.; Holt, J. K.; Stadermann, M.; Grigoropoulos, C. P.; Noy, A.; Bakajin, O. Ion exclusion by sub-2-nm carbon nanotube pores. *Proc. Natl. Acad. Sci. U.S.A.* **2008**, *105*, 17250–17255.

11. Corry, B. Designing carbon nanotube membranes for efficient water desalination. *J. Phys. Chem. B* **2007**, *112*, 1427–1434.

12. Leung, K.; Rempe, S. B.; Lorenz, C. D. Salt permeation and exclusion in hydroxylated and functionalized silica pores. *Phys. Rev. Lett.* **2006**, *96*, 095504-4.

13. Cole, D. R.; Mamontov, E.; Rother, G. Structure and Dynamics of Fluids in Microporous and Mesoporous Earth and Engineered Materials. In *Neutron Applications in Earth, Energy and Environmental Sciences*; Liang, L., Rinaldi, R., Schober, H., Eds.; Springer-Verlag: Berlin, 2009; pp 547–570.

14. Striolo, A.; Chialvo, A. A.; Cummings, P. T.; Gubbins, K. E. Water adsorption in carbon-slit nanopores. *Langmuir* **2003**, *19*, 8583–8591.

15. Striolo, A.; Gubbins, K. E.; Gruszkiewicz, M. S.; Cole, D. R.; Simonson, J. M.; Chialvo, A. A. Effect of temperature on the adsorption of water in porous carbons. *Langmuir* **2005**, *21*, 9457–9467.

16. Wang, J. W.; Kalinichev, A. G.; Kirkpatrick, R. J. Effects of substrate structure and composition on the structure, dynamics, and energetics of water at mineral surfaces: a molecular dynamics modeling study. *Geochim. Cosmochim. Acta* **2006**, *70*, 562–582.

17. Lopes, P. E. M.; Murashov, V.; Tazi, M.; Demchuk, E.; MacKerell, A. D. Development of an empirical force field for silica. Application to the quartz–water interface. *J. Phys. Chem. B* **2006**, *110*, 2782–2792.

18. Nagy, G.; Gordillo, M. C.; Guardia, E.; Marti, J. Liquid water confined in carbon nanochannels at high temperatures. *J. Phys. Chem. B* **2007**, *111*, 12524–12530.

19. Giovambattista, N.; Debenedetti, P. G.; Rossky, P. J. Hydration behavior under confinement by nanoscale surfaces with patterned hydrophobicity and hydrophilicity. *J. Phys. Chem. C* **2007**, *111*, 1323–1332.

20. Shirono, K.; Daiguji, H. Molecular simulation of the phase behavior of water confined in silica nanopores. *J. Phys. Chem. C* **2007**, *111*, 7938–7946.

21. Kerisit, S.; Liu, C. X.; Ilton, E. S. Molecular dynamics simulations of the orthoclase (001)- and (010)-water interfaces. *Geochim. Cosmochim. Acta* **2008**, *72*, 1481–1497.

22. Wander, M. C. F.; Clark, A. E. Structural and dielectric properties of quartz–water interfaces. *J. Phys. Chem. C* **2008**, *112*, 19986–19994.

23. Gordillo, M. C.; Marti, J. Molecular dynamics description of a layer of water molecules on a hydrophobic surface. *J. Chem. Phys.* **2002**, *117*, 3425–3430.

24. Striolo, A. The mechanism of water diffusion in narrow carbon nanotubes. *Nano Lett.* **2006**, *6*, 633–639.

25. Argyris, D.; Tummala, N. R.; Striolo, A.; Cole, D. R. Molecular structure and dynamics in thin water films at the silica and graphite surfaces. *J. Phys. Chem. C* **2008**, *112*, 13587–13599.

26. Argyris, D.; Cole, D. R.; Striolo, A. Dynamic behavior of interfacial water at the silica surface. *J. Phys. Chem. C* **2009**, *113*, 19591–19600.

27. Mamontov, E.; Wesolowski, D. J.; Vlcek, L.; Cummings, P. T.; Rosenqvist, J.; Wang, W.; Cole, D. R. Dynamics of hydration water on rutile studied by backscattering neutron spectroscopy and molecular dynamics simulation. *J. Phys. Chem. C* **2008**, *112*, 12334–12341.

28. Malikova, N.; Cadene, A.; Marry, V.; Dubois, E.; Turq, P. Diffusion of water in clays on the microscopic scale: modeling and experiment. *J. Phys. Chem. B* **2006**, *110*, 3206–3214.

29. Barnette, A. L.; Asay, D. B.; Kim, S. H. Average molecular orientations in the adsorbed water layers on silicon oxide in ambient conditions. *Phys. Chem. Chem. Phys.* **2008**, *10*, 4981–4986.

30. Zhang, Z.; Fenter, P.; Cheng, L.; Sturchio, N. C.; Bedzyk, M. J.; Predota, M.; Bandura, A.; Kubicki, J. D.; Lvov, S. N.; Cummings, P. T.; Chialvo, A. A.; Ridley, M. K.; Benezeth, P.; Anovitz, L.; Palmer, D. A.; Machesky, M. L.; Wesolowski, D. J. Ion adsorption at the rutile-water interface: linking molecular and macroscopic properties. *Langmuir* **2004**, *20*, 4954–4969.

31. Fenn, E. E.; Wong, D. B.; Fayer, M. D. Water dynamics at neutral and ionic interfaces. *Proc. Natl. Acad. Sci. U.S.A.* **2009**, *106*, 15243–15248.

32. Freund, J. B. Electro-osmosis in a nanometer-scale channel studied by atomistic simulation. *J. Chem. Phys.* **2002**, *116*, 2194–2200.

33. Qiao, R.; Aluru, N. R. Ion concentrations and velocity profiles in nanochannel electroosmotic flows. *J. Chem. Phys.* **2003**, *118*, 4692–4701.

34. Yang, K.-L.; Yiacoumi, S.; Tsouris, C. Monte Carlo simulations of electrical double-layer formation in nanopores. *J. Chem. Phys.* **2002**, *117*, 8499–8507.

35. Lima, E. R. A.; Bostrom, M.; Horinek, D.; Biscaia, E. C.; Kunz, W.; Tavares, F. W. Co-ion and ion competition effects: ion distributions close to a hydrophobic solid surface in mixed electrolyte solutions. *Langmuir* **2008**, *24*, 3944–3948.

36. Corry, B. Designing carbon nanotube membranes for efficient water desalination. *J. Phys. Chem. B* **2008**, *112*, 1427–1434.

37. Sint, K.; Wang, B.; Kral, P. Selective ion passage through functionalized graphene nanopores. *J. Am. Chem. Soc.* **2008**, *130*, 16448.

38. Kalra, A.; Garde, S.; Hummer, G. Osmotic water transport through carbon nanotube membranes. *Proc. Natl. Acad. Sci. U.S.A.* **2003**, *100*, 10175–10180.

39. Peter, C.; Hummer, G. Ion transport through membrane-spanning nanopores studied by molecular dynamics simulations and continuum electrostatics calculations. *Biophys. J.* **2005**, *89*, 2222−2234.

40. Lorenz, C. D.; Crozier, P. S.; Anderson, J. A.; Travesset, A. Molecular dynamics of ionic transport and electrokinetic effects in realistic silica channels. *J. Phys. Chem. C* **2008**, *112*, 10222–10232.

41. Shirono, K.; Tatsumi, N.; Daiguji, H. Molecular simulation of ion transport in silica nanopores. *J. Phys. Chem. B* **2009**, *113*, 1041–1047.

42. Kerisit, S.; Ilton, E. S.; Parker, S. C. Molecular dynamics simulations of electrolyte solutions at the (100) goethite surface. *J. Phys. Chem. B* **2006**, *110*, 20491–20501.

43. Marry, V.; Rotenberg, B.; Turq, P. Structure and dynamics of water at a clay surface from molecular dynamics simulation. *Phys. Chem. Chem. Phys.* **2008**, *10*, 4802–4813.

44. Lee, S. H.; Rasaiah, J. C. Molecular dynamics simulation of ion mobility 0.2. Alkali metal and halide ions using the SPC/E model for water at 25 °C. *J. Phys. Chem.* **1996**, *100*, 1420–1425.

45. Koneshan, S.; Rasaiah, J. C. Computer simulation studies of aqueous sodium chloride solutions at 298 K and 683 K. *J. Chem. Phys.* **2000**, *113*, 8125–8137.

46. Sanz, E.; Vega, C. Solubility of KF and NaCl in water by molecular simulation. *J. Chem. Phys.* **2007**, *126*, 014507-13.

47. Du, H.; Rasaiah, J. C.; Miller, J. D. Structural and dynamic properties of concentrated alkali halide solutions: A molecular dynamics simulation study. *J. Phys. Chem. B* **2007**, *111*, 209–217.

48. Schmahl, W. W.; Swainson, I. P.; Dove, M. T.; Graeme-Barber, A. Landau free energy and order parameter behaviour of the ab phase. Transition in cristobalite. *Z. Kristallogr.* **1992**, *201*, 125–145.

49. Puibasset, J.; Pellenq, R. J. M. Grand canonical Monte Carlo simulation study of water structure on hydrophilic mesoporous and plane silica substrates. *J. Chem. Phys.* **2003**, *119*, 9226–9232.

50. Zhuravlev, L. T. The surface chemistry of amorphous silica. Zhuravlev model. *Colloids Surf., A* **2000**, *173*, 1–38.

51. Cygan, R. T.; Liang, J.-J.; Kalinichev, A. G. Molecular models of hydroxide, oxyhydroxide, and clay phases and the development of a general force field. *J. Phys. Chem. B* **2004**, *108*, 1255–1266.

52. Berendsen, H. J. C.; Grigera, J. R.; Straatsma, T. P. The missing term in effective pair potentials. *J. Phys. Chem.* **1987**, *91*, 6269–6271.

53. Miyamoto, S.; Kollman, P. A. SETTLE: an analytical version of the SHAKE and RATTLE algorithm for rigid water models. *J. Comput. Chem.* **1992**, *13*, 952–962.

54. Allen, M. P.; Tildesley, D. J. *Computer Simulation of Liquids*; Oxford University Press: Oxford, 2004.

55. Essmann, U.; Perera, L.; Berkowitz, M. L.; Darden, T.; Lee, H.; Pedersen, L. G. A smooth particle mesh Ewald method. *J. Chem. Phys.* **1995**, *103*, 8577.

56. Smith, D. E.; Dang, L. X. Computer simulations of NaCl association in polarizable water. *J. Chem. Phys.* **1994**, *100*, 3757–3766.

57. Dang, L. X. Free energies for association of Cs$^+$ to 18-crown-6 in water. A molecular dynamics study including counter ions. *Chem. Phys. Lett.* **1994**, *227*, 211–214.

58. Predota, M.; Zhang, Z.; Fenter, P.; Wesolowski, D. J.; Cummings, P. T. Electric double layer at the rutile (110) surface. 2. Adsorption of ions from molecular dynamics and X-ray experiments. *J. Phys. Chem. B* **2004**, *108*, 12061–12072.

59. Nose, S. A Molecular-dynamics method for simulations in the canonical ensemble. *Mol. Phys.* **1984**, *52*, 255–268.

60. Hoover, W. G. Canonical dynamics—equilibrium phase-space distributions. *Phys. Rev. A* **1985**, *31*, 1695–1697.

61. Lindahl, E.; Hess, B.; van der Spoel, D. GROMACS 3.0: a package for molecular simulation and trajectory analysis. *J. Mol. Model.* **2001**, *7*, 306–317.

62. van der Spoel, D.; Lindahl, E.; Hess, B.; Groenhof, G.; Mark, A. E.; Berendsen, H. J. C. GROMACS: fast, flexible, and free. *J. Comput. Chem.* **2005**, *26*, 1701–1718.

63. Hess, B.; Kutzner, C.; vanderSpoel, D.; Lindahl, E. GROMACS 4: algorithms for highly efficient, load-balanced, and scalable molecular simulation. *J. Chem. Theory Comput.* **2008**, *4*, 435–447.

64. Hockney, R. W.; Goel, S. P.; Eastwood, J. W. Quiet high-resolution computer models of a plasma. *J. Comput. Phys.* **1974**, *14*, 148–158.

65. Argyris, D.; Cole, D. R.; Striolo, A. Hydration structure on crystalline silica substrates. *Langmuir* **2009**, *25*, 8025–8035.

66. Puibasset, J.; Pellenq, R. J. M. Water adsorption on hydrophilic mesoporous and plane silica substrates: a grand canonical Monte Carlo simulation study. *J. Chem. Phys.* **2003**, *118*, 5613–5622.

67. Castrillon, S. R. V.; Giovambattista, N.; Aksay, I. A.; Debenedetti, P. G. Effect of surface polarity on the structure and dynamics of water in nanoscale confinement. *J. Phys. Chem. B* **2009**, *113*, 1438–1446.